



**HAL**  
open science

## Structural characterization of the interfacial self-assembly of polyelectrolytes

Revaz Chachanidzea, Kaili Xie, Hanna Massaad, Denis C.D. Roux, Marc Léonetti, Clément de Loubens

► **To cite this version:**

Revaz Chachanidzea, Kaili Xie, Hanna Massaad, Denis C.D. Roux, Marc Léonetti, et al.. Structural characterization of the interfacial self-assembly of polyelectrolytes. 2021. hal-03376419v1

**HAL Id: hal-03376419**

**<https://hal.science/hal-03376419v1>**

Preprint submitted on 13 Oct 2021 (v1), last revised 2 Jun 2022 (v2)

**HAL** is a multi-disciplinary open access archive for the deposit and dissemination of scientific research documents, whether they are published or not. The documents may come from teaching and research institutions in France or abroad, or from public or private research centers.

L'archive ouverte pluridisciplinaire **HAL**, est destinée au dépôt et à la diffusion de documents scientifiques de niveau recherche, publiés ou non, émanant des établissements d'enseignement et de recherche français ou étrangers, des laboratoires publics ou privés.

# STRUCTURAL CHARACTERIZATION OF THE INTERFACIAL SELF-ASSEMBLY OF POLYELECTROLYTES

Supplimentary informations

by R Chachanidze *et al.*

## I. INTERFACIAL RHEOMETRY

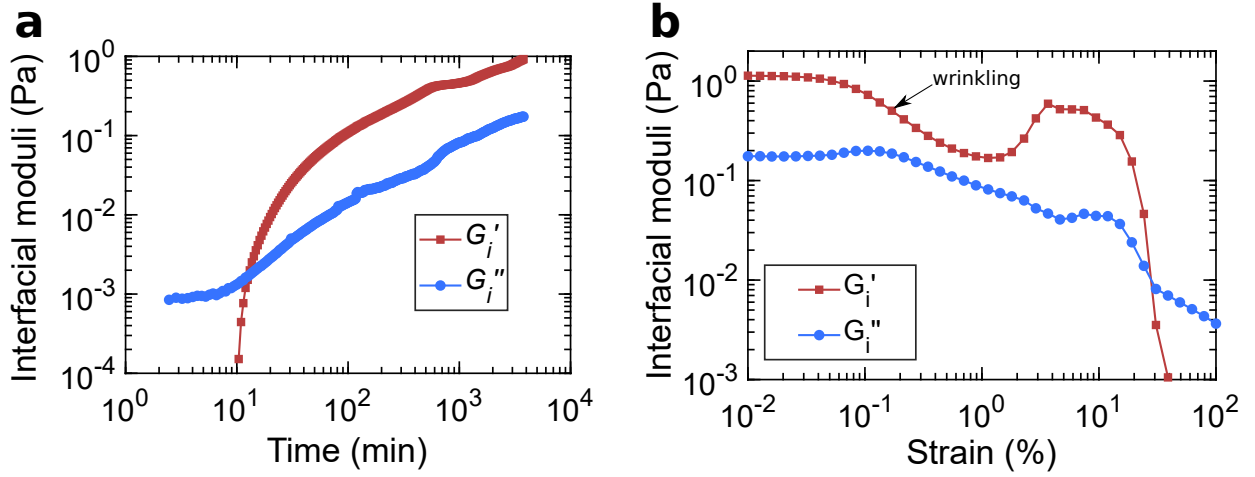


Figure 1: **a:** We performed a long term membrane formation for a single case (0.1% w/w chitosan, 0.1% w/w PFacid ,  $f = 0.5$  Hz,  $\gamma = 0.03\%$ ) in order to perform a strain sweep on a thick membrane and define the limits of linear elastic regime. **B:** We observed that for long term formed membranes ( $>24$  hours) the linear elastic regime was limited to surprisingly low values of strain ( $<0.1\%$ ). The direct microscopic observation of the membrane decorated with tracing particles during the strain sweep experiments showed that this highly non-linear behaviour was caused by wrinkling instability of the membrane. The deformation of  $\approx 20\%$  lead to the rapid decline in  $G'_i$ . The direct observation showed that it was caused by the loss of connectivity between the membrane and the bicone.

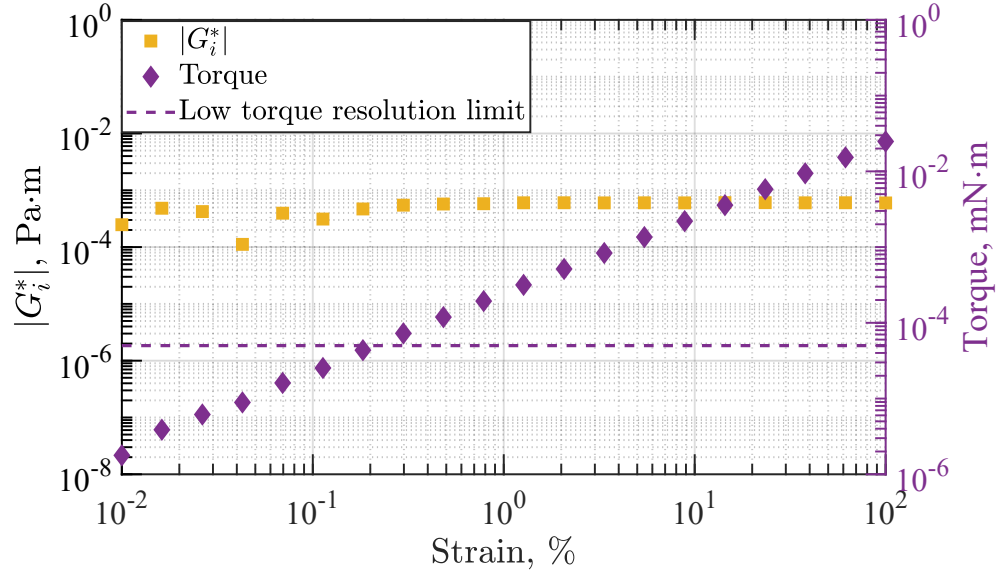


Figure 2: Strain sweep of the chitosan/oil interface. The test was performed with the bicone geometry ( $f = 0.5$  Hz). The aqueous phase contained 0.1% w/w chitosan. PFacid was not added to the oil phase. The result illustrates the steady state chitosan/oil interface without the complexation. **Note:** while the stable values of interfacial viscoelastic modulus  $G_i^*$  are obtained, without the solid membrane forming at the interface the Boussinesq number is very low ( $Bo=0.242$  in this case). Thus this result is qualitative and served as a reference line.

## II. DYNAMIC LIGHT SCATTERING

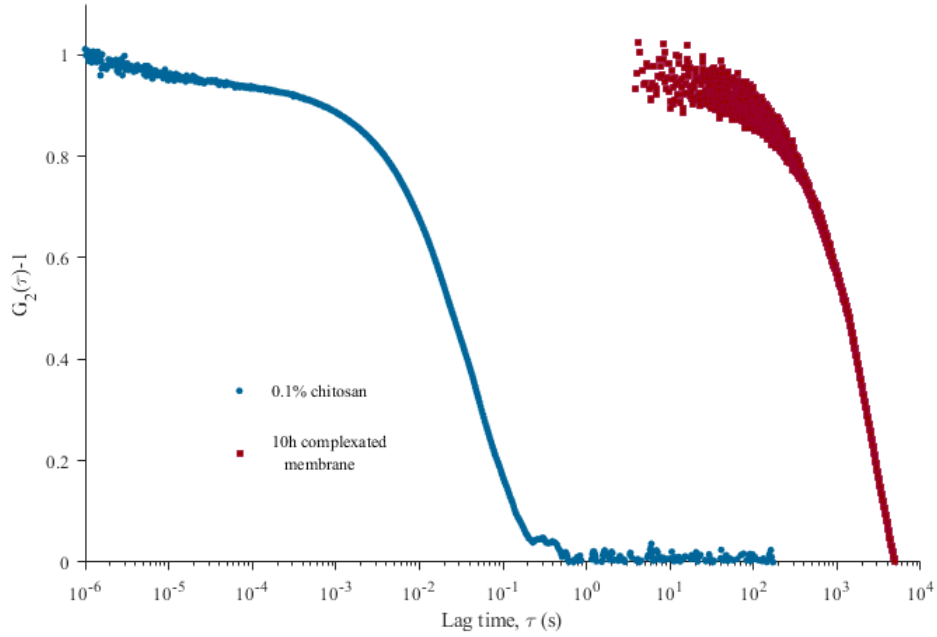


Figure 3: Two distinct cases demonstrating the changes in chitosan/PFAcid membrane DLS signature. The average characteristic relaxation time of chitosan solution (0.1% w/w) was  $\tau = 0.88$  s. The relaxation time of fully formed membrane after 10 hours of complexation was 3488.4 s. Note, that DLS signature of the chitosan solution, being a fast process, was acquired using the PM as a receiver, while the DLS signature of the membrane was acquired with fast camera.

## III. ATOMIC FORCE MICROSCOPY

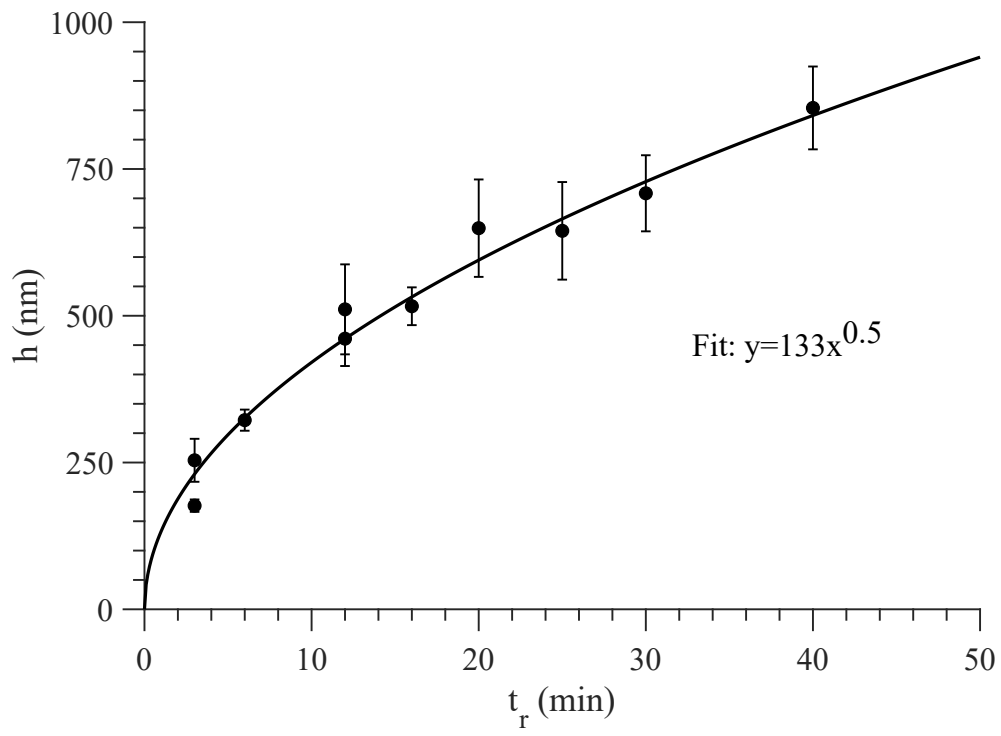
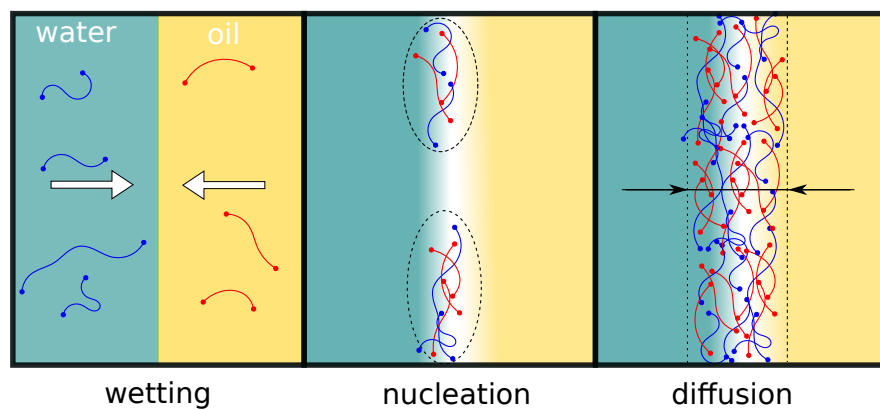


Figure 4

# Graphical Abstract

## Structural characterization of the interfacial self-assembly of polyelectrolytes

Revaz Chachanidze, Kaili Xie, Hanna Massaad, Denis Roux, Marc Leonetti, Clément de Loubens



# Structural characterization of the interfacial self-assembly of polyelectrolytes

Revaz Chachanidze<sup>a,\*</sup>, Kaili Xie<sup>a,b</sup>, Hanna Massaad<sup>a</sup>, Denis Roux<sup>a</sup>, Marc Leonetti<sup>a,c</sup> and Clément de Loubens<sup>a</sup>

<sup>a</sup>Univ. Grenoble Alpes, CNRS, Grenoble INP, LRP, 38000 Grenoble, France

<sup>b</sup>Univ. Bordeaux, CNRS LOMA UMR 5798, Talence F-33405, France

<sup>c</sup>Univ. Aix-Marseille, CNRS, CINaM, Marseille, France

---

## ARTICLE INFO

**Keywords:**  
membrane  
interface  
rheology  
dynamic light scattering

## ABSTRACT

Controlling the assembly of colloids at liquid-liquid interfaces offers new ways to fabricate soft materials with specific physical properties. However, little is known of the relationships between the kinetics of interfacial assembly, structural and rheological properties of such interfaces. We studied the kinetics of the assembly of two oppositely charged polyelectrolytes using a multi-scale approach. Soft interfaces were formed from the complexation at water-oil interface of chitosan, a polysaccharide carrying positively charged groups, and a fatty acid exhibiting negative charges. The growth kinetics of the membrane was followed by interfacial rheometry and space- and time- resolved dynamic light scattering. This set of techniques revealed that the interfacial complexation was a multi-step process. At short time-scale, the interface was fluid and made of heterogeneous patches. At a ‘gelation’ time, the surface elastic modulus and the correlation between speckles increased sharply meaning that the patches percolated. Confocal and electron microscopy confirmed this picture, and revealed that the basic brick of the membrane was sub-micrometric aggregates of polyelectrolytes.

---

## 1. Introduction

Since pioneering observations by Ramsden [1] and Pickering [2] regarding the stabilization of emulsions and foams by colloidal particles trapped at interface, the interfacial assembly of colloids has seen growing interest from scientific communities. It opens the way to the fabrication of materials with specific physical properties such as films, capsules or structured liquids by using interfaces as scaffolds [3] as well as understanding some physiological functions [4]. These materials can be produced by droplet formation [5] or 3D-printing of liquid-liquid interfaces [6]. The main driving mechanism behind the self-assembly of colloids at interface is the process of minimization of interfacial energy, which can be tuned by an external stimulus [7] or by controlling the interactions between the particles [8]. As a result of this assembly, the interface can have a solid-like or liquid-like behaviour. One striking example is the possibility to design mechanically pH-responsive and self-healing microcapsules by interfacial assembly of polymer-polymer coacervates [9], which open the way to *in-situ* reconfigurable structured liquid interfaces.

Building materials based on interfacial assembly of colloids with tuneable properties (e.g. microencapsulation) requires understanding the interplay between the properties of the colloids, the kinetics of interfacial assembly and the resulting properties. For interfaces covered by model nanoparticles [10], the structure of the interface changes with the increasing surface coverage, from a fractal network of aggregates to a heterogeneous structure with voids, to a gel with dense clusters and eventually a densely-packed system [11, 12]. Consequently, viscoelasticity and yield points of these interfaces are controlled by the surface coverage, interparticle interactions and external field forces [12, 13].

H-bond acceptor and donor polymers have also been used to cover water-oil interfaces by interfacial complexation of both polymers [9]. For these systems, the elasticity is controlled by the type and strength of physical interactions [14]. Dupré de Baubigny *et al.* [15] investigated the kinetics of membrane growth on long time scales (> 1,000 s) and identified a diffusion limited process. However, the authors were surprised to observe that the process was faster when polymer molar mass increased. They related this observation to the description of the structure of the membrane as a gel-like porous network, with a pore size much smaller than the radius of the diffusing polymer chains. As a result, the diffusion process should be hindered by the entropic barrier. Another possible approach stabilising interfaces

---

\*Corresponding authors: revaz.chachanidze@univ-grenoble-alpes.fr  
ORCID(s): 0000-0002-4988-9168 (Clément de Loubens)

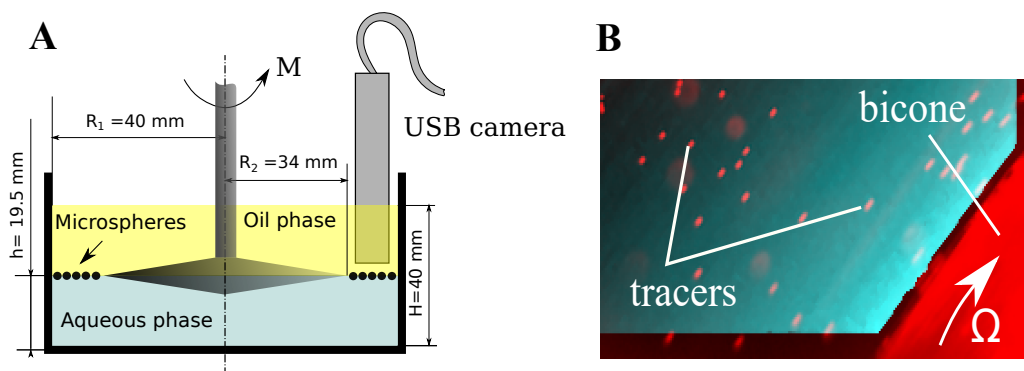


**Figure 1:** Interfacial rheometry by means of IRS. (A) Schematic representation of the bicone rheological cell used to probe the interfacial properties of chitosan / PFacid membrane. The interface was seeded with microparticles to visualize the velocity field of the interface with an immersed camera. (B) PTV at the water-oil interface, the color gradient shows the average velocity of tracers decreasing further when moving away from bicone.

25 is via formation of an interfacial complex whereby two oppositely charged polyelectrolytes are dissolved in different  
 26 immiscible phases. [16, 17, 18, 19, 20, 21]. Upon contact, polycations and polyanions diffuse spontaneously towards  
 27 the interface and form a membrane or a coacervate by electrostatic interactions. As for polymer-polymer interfaces  
 28 [15], membrane growth appears to be limited by the diffusion of one of the polyelectrolytes in the membrane on long  
 29 time scales and membrane elasticity can be controlled with the concentration of polyelectrolytes [17, 21]. Monteillet  
 30 *et al.* [18] studied the kinetics of assembly of polyelectrolytes at water-oil interfaces at macroscopic scales. They  
 31 showed that the assembly was a two-stages process: a fast diffusion limited adsorption process which was followed by  
 32 a much slower logarithmic process. The latter should result from the hindered interpenetration of the two oppositely  
 33 charged polymers, such as coacervation in the bulk [22]. Moreover, self-consistent field analysis carried-out by the  
 34 same group of authors suggested that the coacervate film should be heterogeneous [23]. This latter result highlights  
 35 the importance of structural characterization at colloidal and macroscopic scales in order to describe the formation  
 36 of membrane made of polyelectrolytes complex in relation with their structure and rheological properties. Moreover,  
 37 given the difficulties associated with comparing the results, it is important to combine different methodologies using  
 38 various interfacial characterization tools [24].

39 The aim of our work was to link the kinetics of the assembly of two oppositely charged polyelectrolytes at water-  
 40 oil interface using a multiscale approach. In our study, chitosan, a water soluble cationic polymer, was used to form a  
 41 complex with oil-soluble anionic phosphatidic acids at water-oil interface. This system has been used for microcapsule  
 42 production [17, 21, 25]. However, its interest, for the present study, lies in the fact that the kinetics was relatively slow  
 43 to study the different stage of the assembly of the polyelectrolytes. We characterized the kinetics of assembly at  
 44 macroscopic scales by interfacial rheometer to follow the "gelation" of the interface with measurement of the velocity  
 45 field of the interface. At colloidal scales, we developed space- and time- resolved dynamic light scattering (DLS) to  
 46 characterize the changes in the heterogeneities of the interfaces, which was complemented by confocal and scanning  
 47 electron microscopies (SEM). Lastly, this approach allowed us to relate the structure of the forming film with its  
 48 rheological properties.

## 49 2. Materials and methods

### 50 2.1. Materials

51 Chitosan powder with medium molecular weight and 75-85% deacetylation was purchased from Sigma-Aldrich.  
 52 The anionic surfactant used to complex the chitosan at water-oil interface was phosphatidic fatty acid (PFacid). It was  
 53 comprised of a commercially available lecithin known as lecithin YN (Palsgaard 4448, food-grade, E442, Palsgaard).  
 54 In mass, the phosphatidic acids were 55% w/w, neutral triglycerides 40% and ammonium salts 5%; see [17] for details.  
 55 The molecular structures of both polyelectrolytes are given in Figure 2-A. Sodium hydroxide (1 mol/L) was purchased  
 56 from VWR. The oil-soluble fluorescent dye, Hostasol Yellow 3G (HY-3G), was acquired from Clariant. Rapeseed  
 57 oil (from *Brassica rapa*), hydrochloric acid (36.5-38.0 %, BioReagent, for molecular biology) and cyclohexane (anhy-  
 58 drous, 99.5%) were obtained from Sigma-Aldrich. Deionized water (resistivity > 18 MΩ.cm) was produced from a



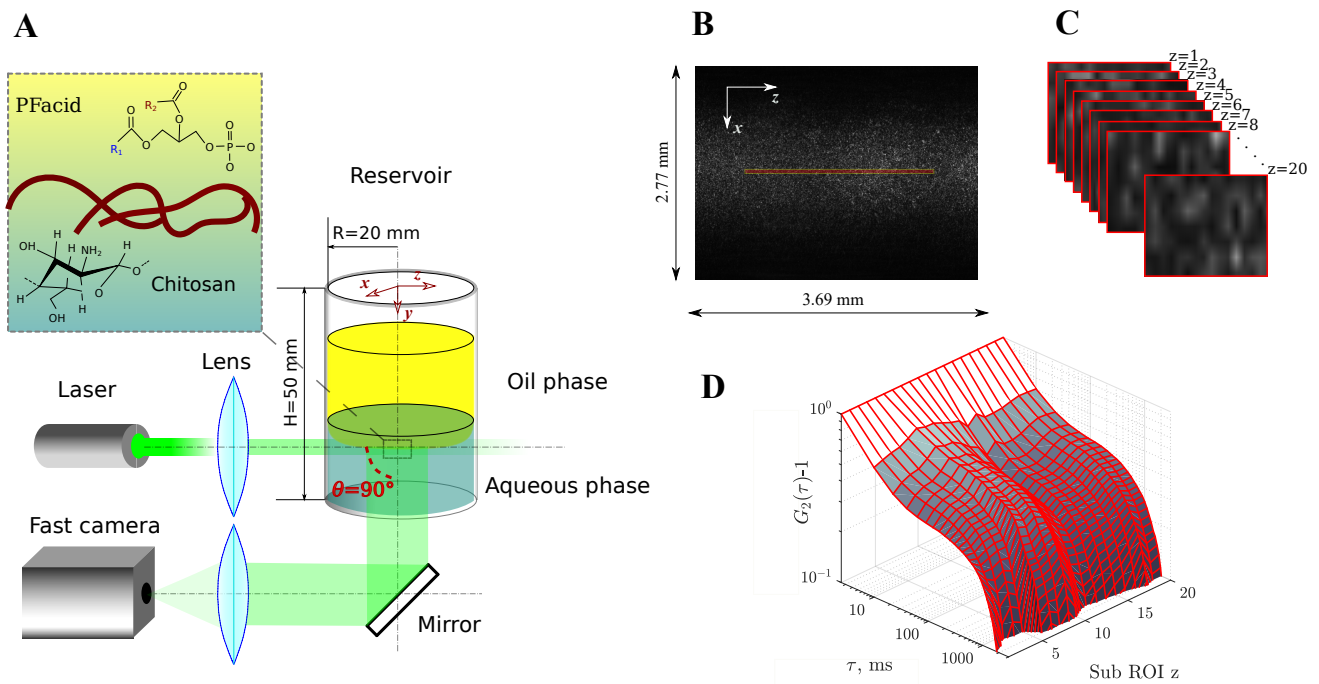


**Figure 2:** Representative sketch of multi-speckles Dynamic Light Scattering. (A) Chitosan / PFAcid membrane was formed at oil-water interface in a cylindrical container. The interface was illuminated by a laser beam set to propagate inside the membrane. The light scattered at  $90^\circ$  was reflected by a polarization holding mirror and collected with a lens onto the camera sensor. (B) Example of an image taken by the CCD camera. In the center, the laser illumination path is clearly visible, showing the speckles. The red rectangle in the middle shows the part of the image used for auto-correlation calculus. (C) Stack representation of the 20<sup>th</sup> sub-ROI obtained by sequencing the red rectangle in B in equisized small images. (D) Intensity correlation function  $g_2 - 1$  as a function of the lag time  $\tau$  and the sub-ROI  $z$ .

59 Millipore Filter water system. CellMask™ Deep Red Plasma membrane stain was obtained from ThermoFisher. All  
 60 chemicals and solvents used in this study were commercially available and used as received unless stated otherwise.

61 The aqueous solution was obtained by dissolving chitosan powder in Millipore water and carefully adjusting the  
 62 pH with hydrochloric acid (1 mol/L) at 3.0 to obtain a solution of 0.1 % w/w. The chitosan solution was then filtered to  
 63 remove undissolved particles through Minisart syringe-filters (pore size 5.0 μm). The viscosity of the 0.1 % chitosan  
 64 solution was 8 mPa·s.

65 The 1 % w/w stock solution of PFAcid was obtained by dissolving lecithin YN overnight in rapeseed oil (carefully  
 66 stirred at  $35^\circ\text{C}$ ). Undissolved particles were removed by centrifugation at  $\times 1000g$  for one hour. The solution was  
 67 the diluted with rapeseed oil to obtain a concentration of PFAcid ranging from 0.1 to 1 % w/w. The viscosity of these  
 68 solutions was  $62.6 \text{ mPa}\cdot\text{s}$  at  $23 \pm 1^\circ\text{C}$ .

## 69 2.2. Interfacial rheometry

70 An interfacial rheological study of a flat film of chitosan / PFAcid complex was performed with a bicone geometry  
 71 using a commercially available solution (**Figure 1**), which is an appropriate approach for interfaces with high moduli  
 72 and viscosities [26]. The Interfacial Rheology System (IRS, Anton Paar, Austria) was mounted on the Modular  
 73 Compact Rheometer MCR 501 (Anton Paar, Austria) after being thoroughly washed with ethanol and Milli-Q water.  
 74 For the interfacial measurements, the bicone geometry was positioned at the height  $H_1 = 19.5 \text{ cm}$  from the bottom of  
 75 the measuring cell after the zero-gap was established. Then the cell was filled with the aqueous phase until the normal  
 76 force acting on the geometry was not adjusted to zero point in order to position the edge of the bicone geometry exactly  
 77 at the interface. Next, the oil phase was gently added over the aqueous phase up to the total height  $H = 40 \text{ cm}$ . Every  
 78 measurement was performed in 3-4 minutes after two phases were brought into contact. All oscillatory measurements  
 79 were performed for at least five time periods per data point. All the measurements were conducted at room temperature  
 80 ( $23 \pm 1^\circ\text{C}$ ).

81 The interfacial viscoelastic properties of the chitosan / PFAcid membrane in oscillatory motion are described by

82 the frequency-dependant complex linear viscoelastic modulus  $G_i^*$ ,

$$G_i^*(\omega) = G_i'(\omega) + iG_i''(\omega) \quad (1)$$

83 where  $G_i'$  and  $G_i''$  are the components of the interfacial complex modulus (two-dimensional elastic modulus and  
84 loss modulus, respectively). It is related to the the complex interfacial viscosity  $\eta_i^*$  as [26]

$$G_i^*(\omega) = i\omega\eta_i^*(\omega) = -\omega\eta_i''(\omega) + i\omega\eta_i'(\omega) \quad (2)$$

85 where  $\eta_i''(\omega)$  is the out-of-phase shear viscosity and  $\eta_i'(\omega)$  is the the dynamic interfacial shear viscosity. The  
86 contributions of the interfacial and bulk components to the torque appearing on the bicone geometry during its motion  
87 were compared through the non-dimensional parameter, the Boussinesq number ( $Bo$ )

$$Bo(\omega) = \frac{\eta_i'(\omega) - i\eta_i''(\omega)}{a(\eta_b^{(1)} + \eta_b^{(2)})} \quad (3)$$

88 where  $\eta_b$  is the bulk viscosity (superscripts denote upper and lower fluid respectively) and  $a$  is the characteristic  
89 length scale that depends on the measuring system. As usual, the interfacial flow was considered to be decoupled from  
90 the bulk. In that case, the interfacial shear viscosity is calculated by [27]:

$$\eta = \frac{M - \frac{8}{3}R_2^3(\eta_b^{(1)} + \eta_b^{(2)})\Omega}{4\pi R_2^2\Omega} \quad (4)$$

91 where  $\Omega$  is the angular velocity (Figure 1 A). This expression is only relevant for the  $Bo \rightarrow \infty$ . For low and  
92 intermediate  $Bo$  a complete analysis must be used, since the influence of the bulk phases becomes important [27].  
93 In our experiments the interfacial response was decoupled from the bulk one by using the Anton Paar application  
94 software.

### 95 2.3. Particle tracking velocimetry

96 The displacements and velocity field on the oil-water interface during rheometric experiments were quantified  
97 through particle tracking velocimetry (PTV). For this purpose, the water-oil interface was decorated at low coverage  
98 with polyethylene microspheres (63-75  $\mu\text{m}$  Cospheric LLC, USA) used as tracers. Less than 0.01% w/w of particle  
99 powder was added to 100 ml of oil phase and mixed thoroughly with a magnetic stirrer overnight. This volume of  
100 oil containing tracers was further used for rheological experiments as described above in the Section 2.2. The USB  
101 microscope (A1 USB Digital Microscope, Andonstar) was immersed in the oil phase during rheological experiments  
102 in IRS in order to visualize the displacement of microspheres under the shear flow. The image sequences were recorded  
103 at 20 frames per second and post-processed with a custom written particle tracking routine (MATLAB, MathWorks).

### 104 2.4. Dynamic light scattering

105 The dynamic evolution of the structure of the membrane was measured by space resolved Dynamic Light Scattering  
106 (DLS) at constant temperature  $T=22^\circ\text{C}$ . A sketch of the custom-built DLS set-up is shown in Figure 2. The oil-  
107 water interface, which later became a membrane, was illuminated by a vertically polarized laser beam produced by a  
108 single-mode laser (MSLIII, CNI, China,  $\lambda = 532 \text{ nm}$ ). The laser beam had a diameter of 2 mm and was shaped by  
109 a combination of two lenses with focal lengths  $f_1 = 200 \text{ mm}$  and  $f_2 = 25.4 \text{ mm}$ . The coherent light was scattered  
110 by forming solid matter at the oil-water interface. Only the light scattered at  $90^\circ$  was collected, after reflection onto  
111 a non-polarized mirror. Focusing the laser beam on the interface was a complicated technical task, as the oil-water  
112 interface formed a concave-convex meniscus depending on the wettability of the cylinder. However the chitosan/PFacid  
113 complexation leading to the membrane formation resulted in a drastic decline in interfacial tension causing the interface  
114 to flatten. This led to the interface displacement along y-axis and consequently signal loss. In order to minimise this  
115 effect, all measurements were performed using a large custom-made glass cylindrical container positioned vertically

116 and sealed underneath with a flat sheet of glass. The dimensions of the reservoir rendered the interface displacement  
 117 negligible and the precise control of the sample volume ensured the tangential contact between the interface and the  
 118 laser beam throughout the experiments.

119 In order to follow the structural evolution of the membrane, the scattered intensity was collected either with a CCD  
 120 camera (acA640-100gm, Basler, Germany) or with a photomultiplier (SPCM-AQR-13, excelitas Technologies, USA).  
 121 When the camera was used, a lens with a focal length  $f_l = 150$  mm allowed the image of the scattering volume to  
 122 form onto the CCD sensor. A diaphragm placed in the focal plane of the lens was set in order to optimize the size of  
 123 the speckles to the pixel size of the camera [28]. For fast processes, the photomultiplier associated with a correlator  
 124 (Flex03-LQ, Correlator.com, USA) was used to widen the dynamic range of acquisition to include lag times as small  
 125 as  $10^{-6}$  s.

126 Our approach enabled nondestructive probing of the interfacial membrane evolution with both spacial and temporal  
 127 resolution, as long as the characteristic relaxation time of the studied system allows signal detection with a digital  
 128 camera. The scattered light detected by CCD camera created the image of a coherence area known as speckle (Figure  
 129 2 B). The red rectangle in the center of the image represents the Region Of Interest (ROI), only this part of the image  
 130 has been used for analysis. This area was sequenced into 20 sub-ROI (Figure 2 C). The individual time autocorrelation  
 131 function of the scattered intensity  $g_2(\tau) - 1$  was computed for each sub-ROI

$$g_2(\tau, z) - 1 = \frac{\langle I^z(t)I^z(t + \tau) \rangle_t}{\langle I^z(t)^2 \rangle_t} - 1 \quad (5)$$

132 where  $I^z(t)$  is the intensity collected within  $z^{th}$  sub-ROI and  $\langle \dots \rangle_t$  denotes averaging over time. Figure 2 D shows  
 133 the result of the intensity correlation function as a function of the sub-ROI  $z$  and the lag time  $\tau$ .

134 We also used the Time Resolved Correlation scheme (TRC) which allows DLS investigation of heterogeneous  
 135 dynamics, as introduced by [29, 30, 31]. Analogously to  $g_2(\tau) - 1$ , the correlation degree  $c_I(t, \tau, z)$  was calculated  
 136 individually for each sub-ROI

$$c_I(t, \tau, z) = \frac{\langle I_p^z(t)I_p^z(t + \tau) \rangle_p}{\langle I_p^z(t) \rangle_p \langle I_p^z(t + \tau) \rangle_p} - 1 \quad (6)$$

137 where  $I_p^z(t)$  is the intensity measured at time  $t$  for the  $p^{th}$  pixel of an image within  $z^{th}$  sub-ROI and  $\langle \dots \rangle_p$  denotes  
 138 averaging over pixels.

## 139 2.5. Microscopy

140 Scanning electron microscopy (SEM) was used to characterize the morphology of chitosan / PFAcid membrane at  
 141 short complexation time. The membranes were grown on the surface of chitosan drops suspended in oil phase which  
 142 contained PFAcid. Once the required complexation time was achieved the droplets were washed in large quantities  
 143 cyclohexane (for more details see [17], [21]) in order to remove the oil with the residues of anionic surfactant. The  
 144 chitosan droplets encapsulated with the membrane were placed on a cover slip and dried at room temperature. Dried  
 145 chitosan / PFAcid membrane were observed by scanning electron microscopy (SEM). Samples were coated with Au/Pd  
 146 in a Baltec MED-020 sputter coater and observed in secondary electron mode in a Thermo Scientific Quanta 250  
 147 microscope equipped with a field emission gun and operating at 2.5 kV.

148 Confocal microscopy was used to characterize the morphology of chitosan / PFAcid membrane at long complexation  
 149 time. Analogously to the SEM characterization described above, the chitosan droplets were injected into oil phase  
 150 containing anionic surfactant. Wet (no cyclohexane washing) chitosan / PFAcid membrane were observed with Leica  
 151 TCS SP8 scanning point confocal microscope equipped with a  $\times 63$  water immersion objective and in-plane image  
 152 resolution  $0.36 \mu\text{m}/\text{px}$ .

## 153 3. Results and discussion

### 154 3.1. Interfacial rheology of chitosan / PFAcid membrane

155 We analysed the kinetics of formation of the membrane with a time sweep experiment at constant amplitude ( $\dot{\gamma} =$   
 156  $0.03\%$ ) and frequency ( $f = 0.5$  Hz). The choice of these parameters was justified by the need to keep the deformation

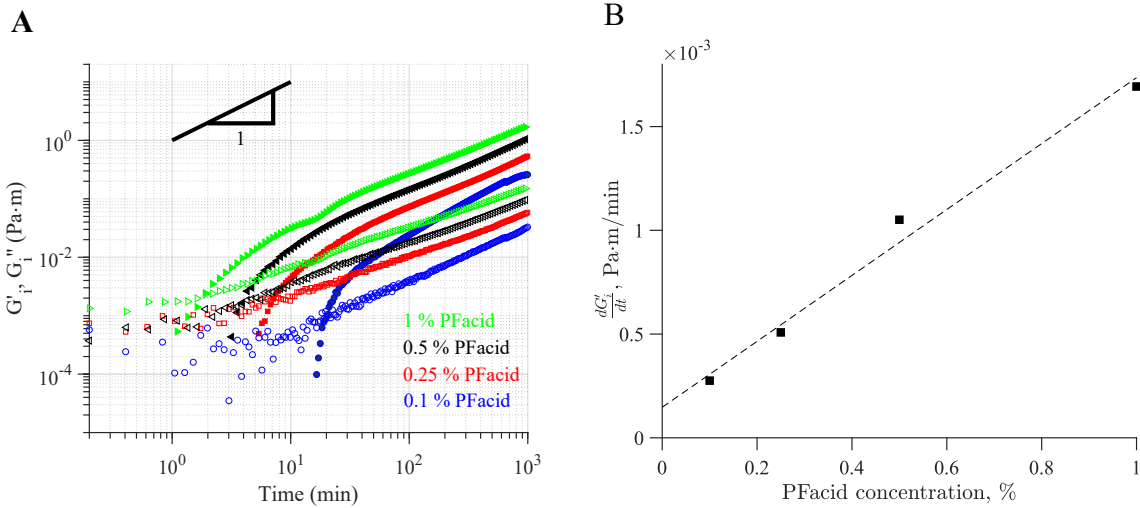


**Figure 3:** Macroscopic study of the interfacial rheological properties of a chitosan / PFacid membrane. (A) Typical time-dependant evolution of interfacial elastic  $G'_i$  and viscous  $G''_i$  shear moduli at different concentrations of PFacid.  $f = 0.5$  Hz,  $\dot{\gamma} = 0.03\%$  Chitosan 0.1% w/w (B) Following a long-term linear regime of membrane, the growth rate of interfacial elastic modulus  $G'_i$ , as a function of anionic surfactant concentration roughly follows a linear law.

157 within the linear viscoelastic regime while maintaining the torque as high as possible (see Figure SI 1). However, as  
 158 explained below, the kinetics depended on the applied strain. Figure 3-A depicts the evolution of  $G'_i$  and  $G''_i$  over time  
 159 for different concentrations of PFacid. As a control, a pure water-oil interface without membrane formation was also  
 160 quantified (see Figure SI 2), which showed a constant  $G''_i$  of  $\sim 10^{-3}$  N/m whereas  $G'_i$  was null. In the early stage of  
 161 membrane formation ( $t < 1$  min for 1% w/w PFacid and 10 min for 0.1% w/w PFacid),  $G''_i$  was almost constant and  
 162 close to the system without PFacid.  $G'_i$  was out of the measurement sensitivity. In this regime, the interface manifested  
 163 purely liquid-like properties. However, within a few minutes, a slow increment in  $G''_i$  was accompanied by a rapid  
 164 growth of  $G'_i$ . The interfacial storage modulus  $G'_i$  quickly overcame  $G''_i$ , manifesting the prevalence of solid-like  
 165 properties. After ten hours of complexation, both interfacial moduli increased on a roughly linearly basis. The atomic  
 166 force microscopy measurements (see **Supporting material**) indicate that the chitosan/PFacid film thickness scales  
 167 with time as  $\sim t^{0.5}$ . Considering that the long term linear development of the interfacial moduli suggests a nonlinear  
 168 relation between interfacial moduli and the membrane thickness.

169 The time for which the interfacial elasticity  $G''_i$  growth abruptly, increased with the concentration of PFacid, Figure  
 170 3-A. Following the initial rapid transition, the growth rate of  $G'_i$  slowed down and increased linearly over time. The  
 171 growth rate of interfacial elastic modulus also scaled on a linear basis with the concentration of PFacid, Figure 3-B.

172 To gain insight into the mechanisms at play in the early moments of membrane formation, creep experiments on the  
 173 forming membrane were coupled to visualisation of the deformation of the interface by PTV (Figure 4). In these creep  
 174 experiments, the bicone geometry was put into motion at fixed torque values and the deformation was measured. As the  
 175 membrane was forming, the shear strain increased gradually until the geometry was brought to arrest. The evolution  
 176 of the deformation varied with the applied torque, Figure 4-A. In analogy with percolation of particle laden interfaces  
 177 [10], we termed the time at which the strain rate was null, the percolation time. The percolation time increased on a  
 178 roughly a linear basis with the applied torque, Figure 4-B. Thus, the percolation process of the interface was coupled  
 179 to the interfacial shear rate. The water-oil interface was decorated at low coverage with polyethylene microspheres ( $\sim$   
 180  $70 \mu\text{m}$ ) used as tracing particles. The radial velocity profile  $v$  of the interface was parabolic during the first few minutes  
 181 of reaction, as expected for liquid interfaces. The spatio-temporal evolution of the velocity shows that the geometry  
 182 slow-down was associated with the flattening of the velocity profile, Figure 4-C,D. Macroscopically, we observed  
 183 that the shear rate tended towards zero in regions closed from the geometry ( $r = 0$  and  $R$ ). However, the velocity  
 184 distribution was strongly heterogeneous before the arrest of the geometry. In fact, a closer look at the interface showed  
 185 a constant formation and rupture of the membrane. We observed small patch-like sheet membranes that grew all over  
 186 the interface and accumulated close to the geometry (see **Supporting video**). When the amount of membrane pieces  
 187 was high enough to fully cover the interface, the interface jammed and stopped the motion of the geometry. This result  
 188 fitted with non-reactive particle laden-interface for which domains of packed particles create elastic interfaces. When

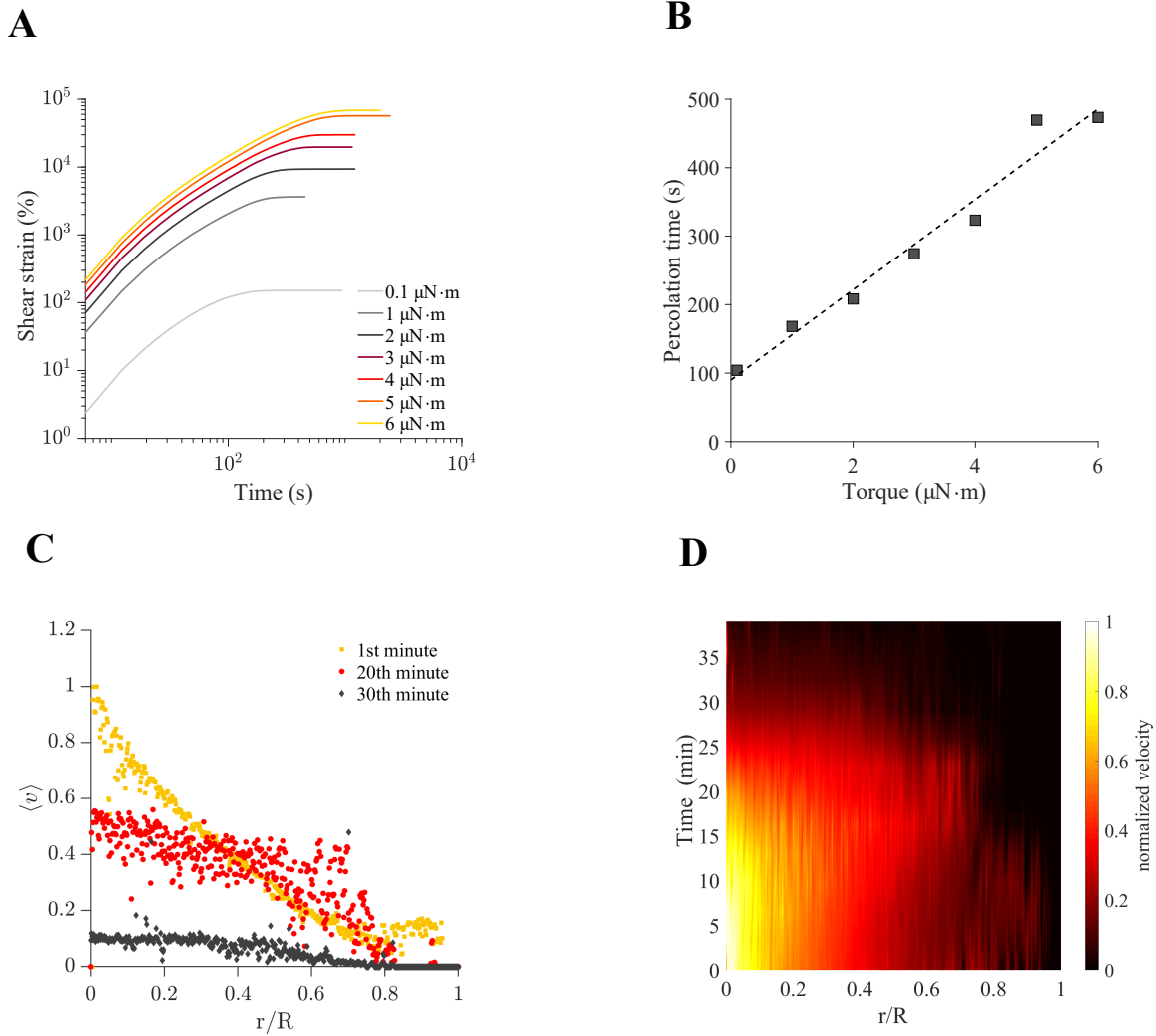


**Figure 4:** Particle tracking on the water-oil interface during the creep experiment. (A) Creep experiments at the water-oil interface during the membrane formation at different torque values. (B) The time required to stop the rotation of the geometry increased on a roughly linear basis with the torque. (C) Normalized velocity profiles at the interface at different stages of membrane formation. (D) The heatmap of normalized velocity values at the different points in time.

189 these domains start to break-up, a transition to viscous-like behavior was observed [32]. Finally, we concluded that  
 190 the complexation of chitosan with PFAcid is a two-step process. At short time scale, the interface has a macroscopic  
 191 rheological behaviour which is characteristic of liquid interfaces, but the interface is strongly heterogeneous and is  
 192 composed of solid patches. At a critical time, called the percolation time, the patches pave the interface and percolated,  
 193 which is macroscopically characterized by a sudden increase of the interfacial elastic modulus  $G'_i$ . At long time scales,  
 194 the thickness of the membrane grew, as  $G'_i$  increased, by diffusion of one of the polyelectrolytes inside the membrane  
 195 [15, 17].

### 196 3.2. Dynamic light scattering experiments

197 In order to shed light on the structural evolution of the interface formation, we employed DLS and TRC analysis  
 198 [29, 30, 33], see Figure 2 for the experimental set-up. The interface was formed at the water-oil interface in a cylindrical  
 199 reservoir via complexation between 0.1% w/w chitosan and 1% w/w PFAcid, Figure 2. During the first 2 s,  $C_I(\tau = 0, t)$   
 200 fluctuated randomly around a steady value of  $\approx 10^{-2}$ , Figure 5. Such behaviour corresponds to a Brownian system  
 201 [29, 31], meaning that the displacement of particles between any two frames was on average the same, independently  
 202 of the complexation time  $t$ . Beyond 2 s, the resolved correlation function drastically increased and gained half a decade  
 203 in 100 s, meaning that the degree of correlation in the sample increased. This behaviour indicated the formation of a

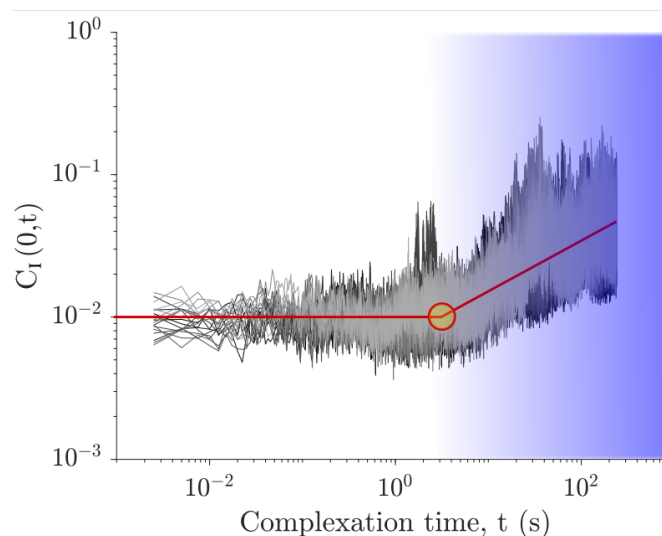


**Figure 5:** Time Resolved Correlation (TRC) at 0 lag time ( $\tau$ ) of building interface of the 20 ROIs. Straights lines are eye-guides and the circle at line interception indicates the starting time of the membrane gelation.

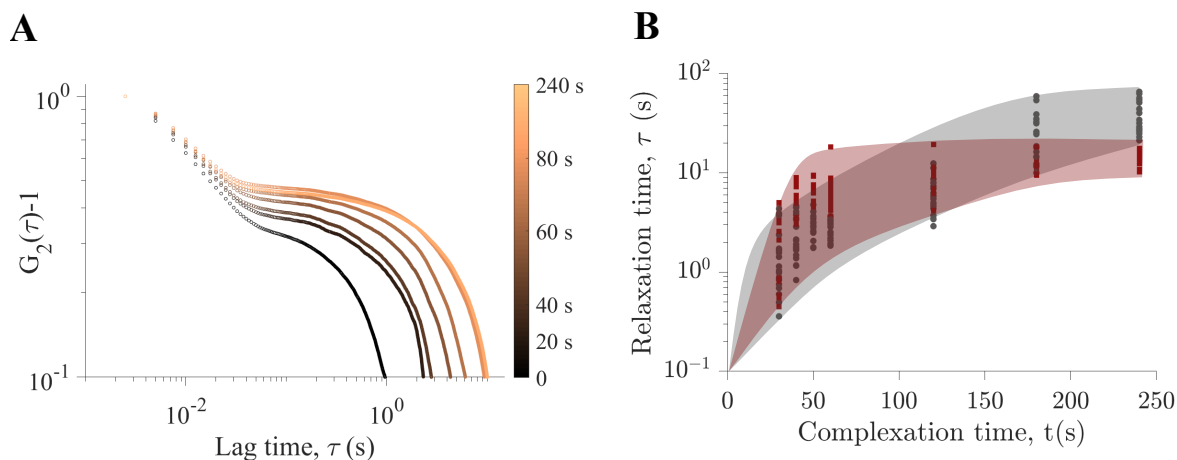


**Figure 6:** (A) Auto-correlation function of the interface computed from the mean time of TRC as at different lag times for an ROI as a function of the time from 0 to 240 s. (B) Evolution of the relaxation times of the forming interface within different sub-ROI computed for two separate experiments at identical conditions. The colored areas separating two experiments serve as guiding lines

204 gel-like interface [29], the result similar to that obtained in rheological study.

205 The kinetics of membrane formation was also probed with the intensity correlation function  $G_2(\tau) - 1$ . Figure 6-A  
 206 shows the intensity correlation function computed at different lag times following the formation time of the membrane  
 207 from 0 to 240 s. At 0 s, the intensity correlation function was identical to the correlation of the chitosan alone (see  
 208 **Supporting material**) with a relaxation time of 0.1 s. As the time increased, a second relaxation time appeared as  
 209 a second mono-exponential function for which relaxation time increased from 0.1 s to more than 10 s in 200 s of mem-  
 210 brane complexation. After long complexation (10 hours), the characteristic relaxation time of a membrane increased  
 211 up to  $2 \times 10^3$  (see **Supporting material**).

212 More interestingly, DLS measurements were also resolved in space, which gave us insight into the formation of  
 213 patches observed during rheological characterisation. The results of spatial analysis are depicted in Figure 6-B, where  
 214 each dot corresponds to an ROI of  $56 \mu\text{m} \times 56 \mu\text{m}$ . Initially, the relaxation time at the interface was the same as that  
 215 of the chitosan. As the chitosan / PFacid complexation took place and a solid matter started to appear at the interface,  
 216 the relaxation time increased. At the different complexation times considered here, the relaxation times differed by  
 217 nearly one decade between different ROI. It indicated high dynamic heterogeneity in the interface complexation. This

218 was consistent with the observation of patches during the interfacial rheological measurement. We concluded that  
219 interfacial complexation of both polyelectrolytes is a spatially heterogeneous process.

### 220 3.3. Scanning electron and confocal microscopy

221 The morphology of chitosan / PFacid membranes formed at relatively short time scales was observed by Scanning  
222 electron microscopy (SEM). In order to minimise harsh manipulations with fragile membranes, chitosan / PFacid  
223 membranes were grown on a surface of water droplets in oil phase containing chitosan and PFacid respectively, for  
224 more details see [21]. The complexation reaction was stopped by a gentle washing in large quantities of cyclohexane.  
225 After that, the droplets now enclosed by a solid membrane were placed on the glass substrate and dried prior the SEM  
226 imaging.

227 Figure 7 demonstrates the morphology of the chitosan / PFacid formed at 0.5 and 2 min of complexation time.  
228 The short time formed membrane was characterized by an important heterogeneity of its structure (Figure 7 A). The  
229 membrane appeared to be formed out of a large number of non-connected patches of 1-5  $\mu\text{m}$ . Additionally, large non-  
230 circular holes up to 10  $\mu\text{m}$  were found in the membrane. At 2 minutes of complexation the interface appeared to be  
231 fully formed, except for the presence of large circular holes (Figure 7 B). Figure 7 C shows the transversal view of the  
232 membrane, which was characterized by sub-micrometric aggregates.

233 The confocal imaging was carried out on the thick membrane after 48h of complexation in order to reveal the  
234 internal structure of the interface. Water droplets containing 0.1 % w/w concentration of chitosan were injected into  
235 the oil phase containing 0.1 % w/w concentration of PFacid. Water-soluble fluorescent dye with high lipid affinity  
236 (CellMask™ Deep Red plasma membrane stain, Invitrogen™) was added to the aqueous phase. This dye has little to  
237 no fluorescence in a free form and is only fluorescent once it is "anchored" to lipids. Figure 7 depicts the results of  
238 confocal imaging. These images show that the membrane was composed of nano-metric inclusions. Figure 7-right  
239 shows the concentration gradient of these inclusions from the oil phase towards the aqueous phase. As the fluorescent  
240 dye anchored to lipids, we deduced that this gradient of light intensity corresponds to a gradient of PFacid.

241 This set of microscopy images consolidated the idea that membrane formation was due to the percolation of in-  
242 dividual patches. When the patches were able to form a percolated network, large holes were present. These results  
243 were reminiscent of interfaces covered by model nanoparticles which form heterogeneous structures with voids for  
244 low particle surface coverage [12, 11, 10]. The basic bricks are sub-micrometric aggregates of polyelectrolytes. On  
245 long time scales, the membrane was fully covered of these aggregates. In the thickness of the membrane, there was a  
246 negative gradient of these aggregates from the oil phase to the water phase. This last result supports the idea that the  
247 growth of the membrane was limited by the diffusion through a gel-like porous network of PFacid on long time scales,  
248 as described for H-bond donor / acceptor polymers [15].

## 249 4. Conclusion

250 Membrane formation based on the complexation between chitosan and short chain fatty acid has been used as  
251 a model for interfacial self-assembly of poly-electrolytes. A multi-scale approach was used in order to perform a  
252 characterisation of membrane formation and morphology.

253 The rheological properties of the forming membrane at macroscopic scale were probed by a combination of inter-  
254 facial rheometry using the bicone geometry and particle tracking velocimetry of the interface. On short time scales, the  
255 interface had a fluid-like behaviour and was composed of non-connected solid patches. The elastic behaviour emerged  
256 when the patches percolated, similarly to a particle laden interface with an increasing surface coverage [13, 12, 10].  
257 On long time scales, the surface elasticity increased almost linearly with time and concentration of the short chain fatty  
258 acid. This regime was reminiscent of a membrane growth limited by the diffusion of the smallest entity of both com-  
259 plexing molecules, as observed for polymer membranes obtained by h-bonding [9, 14, 15]. This finding was supported  
260 by confocal imaging showing a concentration gradient of short chain fatty acid through the membrane.

261 The membrane formation is a two step process. First the interfacial reaction takes place and is governed by the  
262 reactivity of the interacting species. Then the reaction takes place in the membrane and is limited by the diffusion  
263 through the interfacial membrane. We employed several techniques in order to characterize these processes at different  
264 scales. At microscopic scales, we characterized the structure of the interface by space- and time- resolved DLS, used  
265 up to now in bulk for gels [33, 31, 29]. The method demonstrated that membrane formation was strongly heterogeneous  
266 in space and confirmed that was a two step process. On short time-scale, the speckles were strongly non-correlated,  
267 meaning that the interface had a fluid-like behaviour. On long time scales, the correlation of the speckles increased,

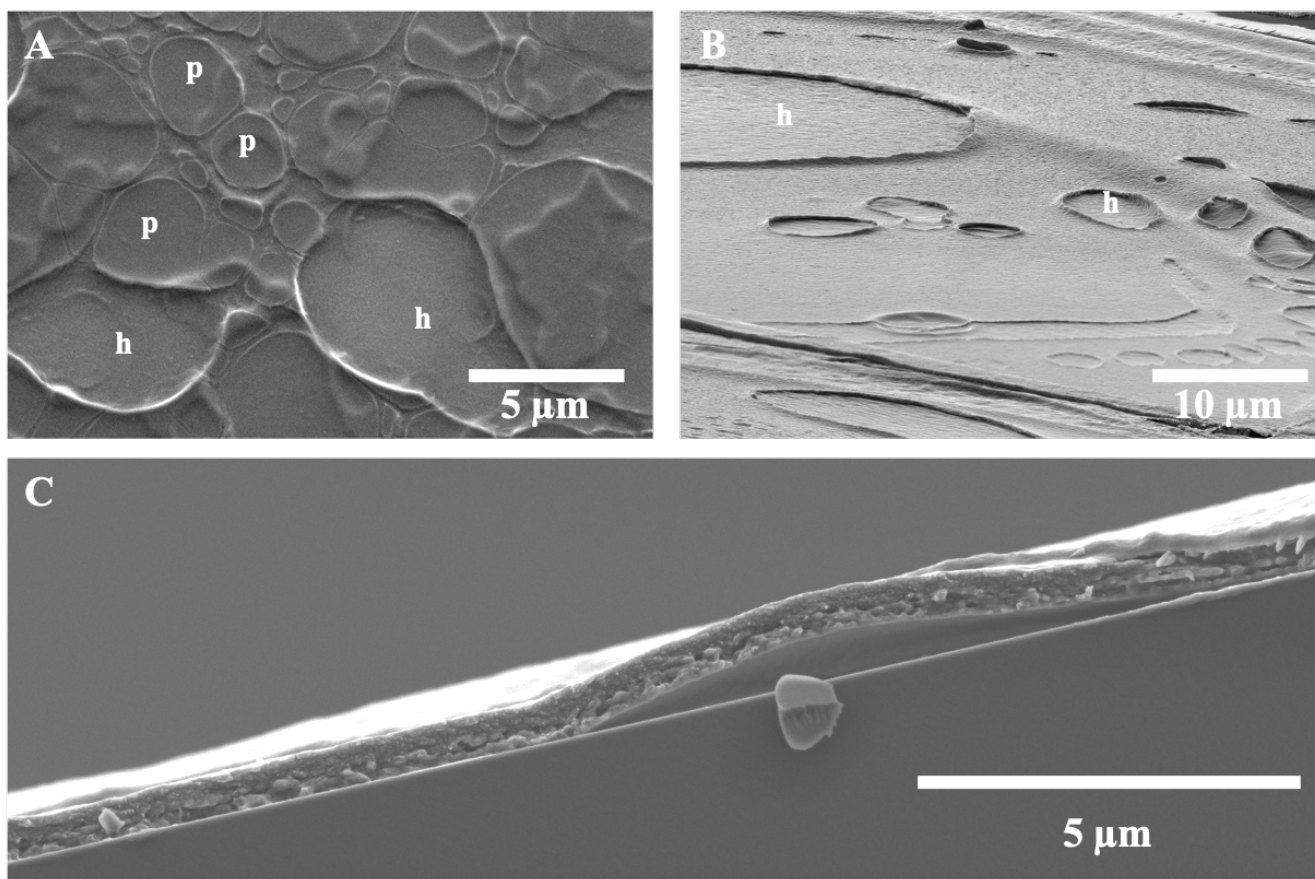


**Figure 7:** SEM images of dried chitosan / PFacid membrane. (A) CH / PFacid membrane after 30 s of complexation. The interface was made of individual patches of 1-50  $\mu\text{m}$  size (p), as well as large holes (h). (B) CH / PFacid membrane after 2 min of complexation. The interface was homogeneous, with the exception of circular holes (h). (C) View in the thickness of the membrane after 2 min of complexation. The membrane showed a granular structure.

268 as a sign of the gelation of the interface. The strong spatial heterogeneity was consistent with a process of membrane  
 269 growth due to the formation of nuclei and then their percolation to form a gel. The employed method allows the  
 270 dynamic and non-destructive measurement of the forming film without stopping the reaction.

271 Some of the other types of interfacial polymerization reactions that proved to be very interesting for industrial  
 272 applications (such as polyamide, polyurethane, polyurea and etc. membranes) were studied extensively [34]. For these  
 273 reaction types the membrane growth was confirmed to take place in organic phase. We however observed the smaller  
 274 anionic surfactant to diffuse through the membrane into the aqueous phase. SEM and confocal imaging confirmed  
 275 the presence of microscopic patches and showed also that the basic bricks were sub-micrometric aggregates of poly-  
 276 electrolytes. When the interface was fully covered with these aggregates, the membrane grew in its thickness by a  
 277 diffusion-like process of the short chain fatty acid. This finding was supported by the growth of the elastic modulus  
 278 with the concentration of PFacid and the gradient of PFacid in the thickness of the membrane.

279 Finally, this multi-scale experimental approach created a robust overarching picture of the interfacial complexation  
 280 of polyelectrolytes. At short time scales, the growth is limited by the formation of "nuclei" which form patches. This  
 281 work brings new elements on interfacial complexation that should prove useful to control the properties of liquid-liquid  
 282 interfaces for the design of new materials, such as microcapsules or structured liquids.

## 283 5. Acknowledgements

284 LRP is part of the LabEx Tec21 (ANR-11-LABX-0030) and of the PolyNat Carnot Institute (ANR-11-CARN-007-  
 285 01). The authors express their sincere gratitude to Christine Lancelon-Pin (CERMAV-CNRS, Grenoble, France) for  
 286 her assistance with scanning-electron microscopy. The authors acknowledge the NanoBio-ICMG chemistry platform



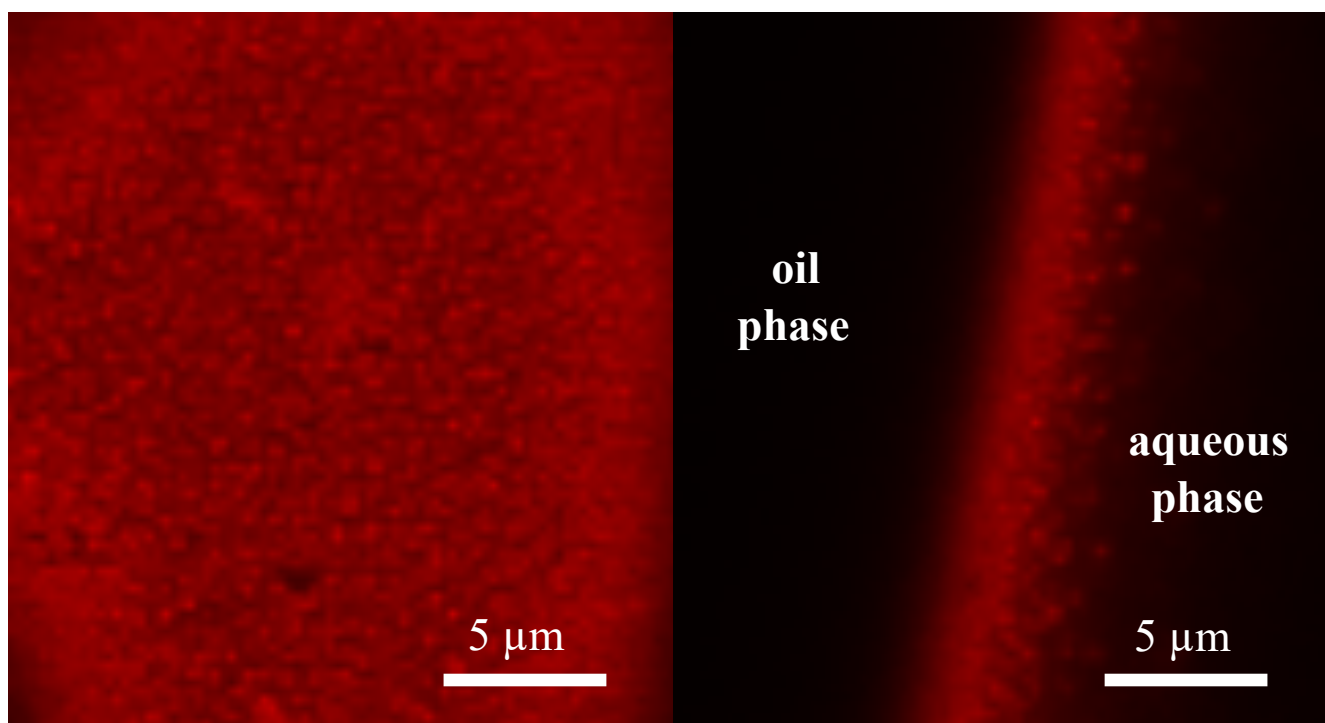


**Figure 8:** Confocal images of wet Chitosan / PFacid membrane after 48h of complexation. The membrane was marked by a fluorescent dye with lipid affinity (see text for details). Left: A piece of a membrane laying flat on a glass substrate showing a granularly patterned structure. Right: A horizontal confocal slice of a labeled membrane.

287 (UAR 2607, Grenoble) for granting access to the electron microscopy facilities. The authors thank the support of ANR  
 288 2DVisc (ANR-18-CE06-0008-01).

## 289 6. Author contributions

290 **Revaz Chachanidze:** Conceptualization, Methodology, Formal analysis, Investigation, Writing - Original Draft,  
 291 Visualization **Kailie Xie:** Conceptualization, Methodology, Investigation, Writing - Review & Editing **Hanna Mas-**  
 292 **sad:** Methodology, Formal analysis, Investigation, Writing - Original Draft, Visualization **Denis Roux:** Methodology,  
 293 Formal analysis, Writing - Original Draft, Supervision **Marc Leonetti:** Conceptualization, Methodology, Writing -  
 294 Original Draft, Supervision **Clément de Loubens:** Conceptualization, Methodology, Writing - Original Draft, Super-  
 295 vision

## 296 References

- 297 [1] W. Ramsden, Separation of solids in the surface-layers of solutions and ‘suspensions’ (observations on surface-membranes, bubbles, emulsions,  
 298 and mechanical coagulation).—preliminary account, Proceedings of the royal Society of London 72 (477-486) (1904) 156–164.  
 299 [2] S. U. Pickering, Cxciv.—the interaction of metallic sulphates and caustic alkalis, Journal of the Chemical Society, Transactions 91 (1907)  
 300 1981–1988.  
 301 [3] J. Forth, P. Y. Kim, G. Xie, X. Liu, B. A. Helms, T. P. Russell, Building reconfigurable devices using complex liquid–fluid interfaces, Advanced  
 302 Materials 31 (18) (2019) 1806370.  
 303 [4] P. Bertsch, J. Bergfreund, E. J. Windhab, P. Fischer, Physiological fluid interfaces: Functional microenvironments, drug delivery targets, and  
 304 first line of defense, Acta Biomaterialia (2021).  
 305 [5] E. Amstad, Capsules: Their past and opportunities for their future (2017).  
 306 [6] R. Xu, T. Liu, H. Sun, B. Wang, S. Shi, T. P. Russell, Interfacial assembly and jamming of polyelectrolyte surfactants: A simple route to print  
 307 liquids in low-viscosity solution, ACS Applied Materials & Interfaces 12 (15) (2020) 18116–18122.  
 308 [7] A. Maestro, Tailoring the interfacial assembly of colloidal particles by engineering the mechanical properties of the interface, Current opinion  
 309 in colloid & interface science 39 (2019) 232–250.  
 310 [8] J. N. Israelachvili, Intermolecular and surface forces, Academic press, 2015.  
 311 [9] J. D. de Baubigny, C. Trégouët, T. Salez, N. Pantoustier, P. Perrin, M. Reyssat, C. Monteux, One-step fabrication of ph-responsive membranes  
 312 and microcapsules through interfacial h-bond polymer complexation, Scientific reports 7 (1) (2017) 1–7.

- 313 [10] J. H. Thijssen, J. Vermant, Interfacial rheology of model particles at liquid interfaces and its relation to (bicontinuous) pickering emulsions,  
314 Journal of Physics: Condensed Matter 30 (2) (2018) 023002.
- 315 [11] S. Reynaert, P. Moldenaers, J. Vermant, Interfacial rheology of stable and weakly aggregated two-dimensional suspensions, Physical Chemistry  
316 Chemical Physics 9 (48) (2007) 6463–6475.
- 317 [12] K. Masschaele, J. Franssaer, J. Vermant, Direct visualization of yielding in model two-dimensional colloidal gels subjected to shear flow,  
318 Journal of rheology 53 (6) (2009) 1437–1460.
- 319 [13] M. Cui, T. Emrick, T. P. Russell, Stabilizing liquid drops in nonequilibrium shapes by the interfacial jamming of nanoparticles, Science  
320 342 (6157) (2013) 460–463.
- 321 [14] S. Le Tirilly, C. Tregouët, S. Bône, C. Geffroy, G. Fuller, N. Pantoustier, P. Perrin, C. Monteux, Interplay of hydrogen bonding and hydrophobic  
322 interactions to control the mechanical properties of polymer multilayers at the oil–water interface, ACS Macro Letters 4 (1) (2015) 25–29.
- 323 [15] J. Dupré de Baubigny, P. Perrin, N. Pantoustier, T. Salez, M. Reyssat, C. Monteux, Growth mechanism of polymer membranes obtained by  
324 h-bonding across immiscible liquid interfaces, ACS Macro Letters 10 (2) (2021) 204–209.
- 325 [16] D. Grigoriev, T. Bukreeva, H. Möhwald, D. Shchukin, New method for fabrication of loaded micro- and nanocontainers: emulsion encapsulation  
326 by polyelectrolyte layer-by-layer deposition on the liquid core, Langmuir 24 (3) (2008) 999–1004.
- 327 [17] D. Z. Gunes, M. Pouzot, M. Rouvet, S. Ulrich, R. Mezzenga, Tuneable thickness barriers for composite o/w and w/o capsules, films, and their  
328 decoration with particles, Soft Matter 7 (19) (2011) 9206–9215.
- 329 [18] H. Monteillet, F. Hagemans, J. Sprakel, Charge-driven co-assembly of polyelectrolytes across oil–water interfaces, Soft Matter 9 (47) (2013)  
330 11270–11275.
- 331 [19] G. Kaufman, R. Boltyskiy, S. Nejadi, A. R. Thiam, M. Loewenberg, E. R. Dufresne, C. O. Osuji, Single-step microfluidic fabrication of soft  
332 monodisperse polyelectrolyte microcapsules by interfacial complexation, Lab on a Chip 14 (18) (2014) 3494–3497.
- 333 [20] M. Kim, S. J. Yeo, C. B. Highley, J. A. Burdick, P. J. Yoo, J. Doh, D. Lee, One-step generation of multifunctional polyelectrolyte microcapsules  
334 via nanoscale interfacial complexation in emulsion (nice), ACS nano 9 (8) (2015) 8269–8278.
- 335 [21] K. Xie, C. de Loubens, F. Dubreuil, D. Z. Gunes, M. Jaeger, M. Leonetti, Interfacial rheological properties of self-assembling biopolymer  
336 microcapsules, Soft matter 13 (36) (2017) 6208–6217.
- 337 [22] E. Spruijt, J. Sprakel, M. Lemmers, M. A. C. Stuart, J. van der Gucht, Relaxation dynamics at different time scales in electrostatic complexes:  
338 Time-salt superposition, Phys. Rev. Lett. 105 (2010) 208301. doi:10.1103/PhysRevLett.105.208301.  
339 URL <https://link.aps.org/doi/10.1103/PhysRevLett.105.208301>
- 340 [23] H. Monteillet, J. Kleijn, J. Sprakel, F. Leermakers, Complex coacervates formed across liquid interfaces: A self-consistent field analysis,  
341 Advances in colloid and interface science 239 (2017) 17–30.
- 342 [24] M. D. Biviano, L. J. Böni, J. D. Berry, P. Fischer, R. R. Dagastine, Viscoelastic characterization of the crosslinking of  $\beta$ -lactoglobulin on  
343 emulsion drops via microcapsule compression and interfacial dilational and shear rheology, Journal of Colloid and Interface Science 583  
344 (2021) 404–413.
- 345 [25] M. Maleki, C. de Loubens, K. Xie, E. Talansier, H. Bodiguel, M. Leonetti, Membrane emulsification for the production of suspensions of  
346 uniform microcapsules with tunable mechanical properties, Chemical Engineering Science 237 (2021) 116567.
- 347 [26] D. Renggli, A. Aliche, R. H. Ewoldt, J. Vermant, Operating windows for oscillatory interfacial shear rheology, Journal of Rheology 64 (1)  
348 (2020) 141–160.
- 349 [27] P. Erni, P. Fischer, E. J. Windhab, V. Kusnezov, H. Stettin, J. Läger, Stress- and strain-controlled measurements of interfacial shear viscosity  
350 and viscoelasticity at liquid/liquid and gas/liquid interfaces, Review of Scientific Instruments 74 (11) (2003) 4916–4924. arXiv:<https://doi.org/10.1063/1.1614433>, doi:10.1063/1.1614433.  
351 URL <https://doi.org/10.1063/1.1614433>
- 352 [28] N. Ali, Rhéospeckle : un nouvel outil d'étude du comportement multi-échelle des matériaux hétérogènes, Ph.D. thesis, Université Grenoble  
353 Alpes, thèse de doctorat dirigée par Roux, Denis et Caton, François (2016).  
354 URL <http://www.theses.fr/2016GREAI013>
- 355 [29] L. Cipelletti, H. Bissig, V. Trappe, P. Ballesta, S. Mazoyer, Time-resolved correlation: a new tool for studying temporally heterogeneous  
356 dynamics, Journal of Physics: Condensed Matter 15 (1) (2002) S257.
- 357 [30] H. Bissig, S. Romer, L. Cipelletti, V. Trappe, P. Schurtenberger, Intermittent dynamics and hyper-aging in dense colloidal gels, PhysChem-  
358 Comm 6 (5) (2003) 21–23.
- 359 [31] A. Duri, H. Bissig, V. Trappe, L. Cipelletti, Time-resolved-correlation measurements of temporally heterogeneous dynamics, Phys. Rev. E 72  
360 (2005) 051401. doi:10.1103/PhysRevE.72.051401.  
361 URL <https://link.aps.org/doi/10.1103/PhysRevE.72.051401>
- 362 [32] S. Barman, G. F. Christopher, Role of capillarity and microstructure on interfacial viscoelasticity of particle laden interfaces, Journal of  
363 Rheology 60 (1) (2016) 35–45.
- 364 [33] E. Secchi, T. Roversi, S. Buzzaccaro, L. Piazza, R. Piazza, Biopolymer gels with “physical” cross-links: gelation kinetics, aging, heterogeneous  
365 dynamics, and macroscopic mechanical properties, Soft Matter 9 (15) (2013) 3931–3944.
- 366 [34] C. Perignon, G. Ongmayeb, R. Neufeld, Y. Frere, D. Poncelet, Microencapsulation by interfacial polymerisation: Membrane formation and  
367 structure, Journal of microencapsulation 32 (2014) 1–15. doi:10.3109/02652048.2014.950711.  
368